Optim Eng (2012) 13:57–78
DOI 10.1007/s11081-011-9159-x

Topology optimization using the finite cell method

J. Parvizian · A. Düster · E. Rank

Received: 14 May 2009 / Accepted: 26 May 2011 / Published online: 1 July 2011

Abstract Huge effort has been spent over the past decades to develop efficient numerical methods for topology optimization of mechanical structures. Most recent investigations have focused on increasing the efficiency and robustness, improving the optimization schemes and extending them to multidisciplinary objective functions. The vast majority of available methods is based on low order finite elements, assuming one element as the smallest entity which can be assigned material in the optimization process. Whereas the present paper uses only a very simple, heuristic optimization procedure, it investigates in detail the feasibility of high order elements for topology optimization. The *Finite Cell Method*, an extension of the p-version of FEM is used, which completely separates between the description of the geometry of a structure and *cells*, where the high order shape functions are defined. Whereas geometry is defined on a (very) fine mesh, the *material grid*, shape functions live on a much coarser grid of elements, the finite cells. The method takes advantage of the ability of high order elements to accurately approximate even strongly inhomogeneous material distribution *within one element* and thus boundaries between material and void which pass through the interior of the coarse cells. Very attractive properties

This work is the result of an institutional partnership of the three authors being supported by the Alexander von Humboldt Foundation. This support is gratefully acknowledged.

J. Parvizian (✉)
Department of Industrial Engineering, Isfahan University of Technology, Isfahan, 84156 83111, Iran
e-mail: japa@cc.iut.ac.ir

A. Düster
Numerische Strukturanalyse mit Anwendungen in der Schiffstechnik (M-10), Technische Universität Hamburg-Harburg, Schwarzenbergstr. 95c, 21073 Hamburg, Germany
e-mail: alexander.duester@tu-harburg.de

E. Rank
Chair for Computation in Engineering, Faculty of Civil Engineering and Geodesy, Technische Universität München, Arcisstr. 21, 80333 Munich, Germany
e-mail: rank@bv.tum.de

of the proposed method can be observed: Due to the high order approach the stress field in the optimized structure is approximated very accurately, no checkerboarding is observed, the iteratively found boundary of the structure is very smooth and the observed number of iterations is in general very small.

Keywords Topology optimization · Finite cell method

1 Introduction

Topology optimization for the minimum compliance and a constrained weight is in a mature stage of technology, where a significant number of commercial software tools are available and many industrial applications have been established. Excellent surveys on methods and applications are provided, for example, by Eschenauer and Olhoff (2001) and Bendsøe and Sigmund (1995, 2004). Even though, increasing the efficiency of optimization procedures is still a major field of attraction for research activities (Andreassen et al. 2010; Challis 2010; Huang and Xie 2010; Tang et al. 2010).

Central to all approaches is a method to define and modify the topology of the structure to be optimized. The topology can be changed either by inserting holes in the body, that may vary in size or even merge (Eschenauer et al. 1994; Parvizian and Fenner 1997), or by changing the density of the material in different regions, so that a zero or low density defines a void in the body. Since a different number of holes may lead to different (locally) optimal solutions, insertion of initial holes has not been broadly investigated during the last decade, although the basic idea has gained attention recently in the *level set* literature as a trigger for the topology optimization procedure (Sethian and Wiegmann 2000; Allaire et al. 2004; Allaire and Jouve 2006).

An alternative way to change the topology of a structure has been followed in many different, yet similar *element based* approaches. They all modify the material density in each element during the optimization process according to its role in bearing the load determined by the equivalent stresses or, more general, the role the element has in changing the objective function determined by a sensitivity analysis. Therefore, each element can have a constant density in a range starting from zero to some positive value, while zero density means a void element—the *soft kill* technique. In the alternative *hard kill* technique (Xie and Steven 1997; Huang and Xie 2010), the density of each element can have only two discrete values, either *zero* for a void or *the density* of the material used. A total removal of elements introduces corners and may thus cause artificial singularities that effect the decision taken in the next steps based on the stress levels, see Fig. 1a. So far, most algorithms ignore such singularities, arguing that they do not have any physical meaning. However, this makes it difficult to report an accurate stress distribution in a body optimized this way. The *hard kill* technique also may result in non-admissible topologies (Zhou and Rozvany 2001), if void elements detach an essential boundary totally from the support (Huang and Xie 2008). A review on stress-based topology optimization can be found in Le et al. (2010).

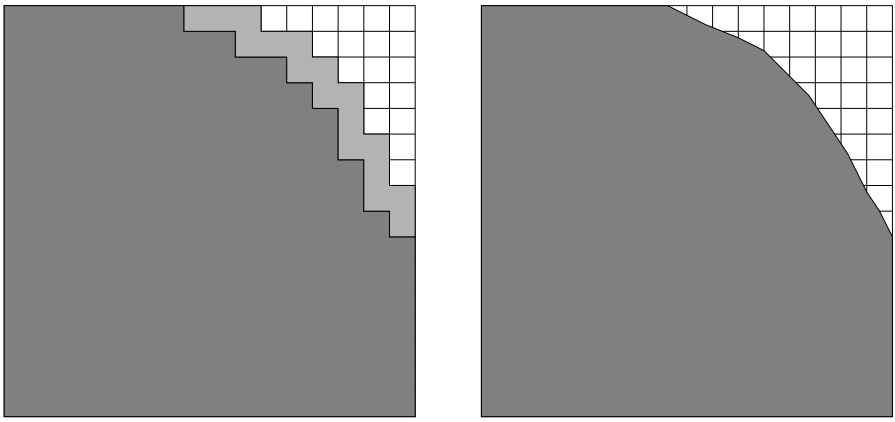

Fig. 1 (**a**) (*left*) In most element based topology optimization the boundary moves according to the elements. (**b**) (*right*) In the cell-based algorithm, cells can be cut by a polygonal boundary defining the interface between material and void region

Homogenization techniques assume that elements are made of composite materials and determine the stiffness based on homogenization analysis of the material (Bendsøe 1995; Bendsøe and Sigmund 2004; Bendsøe et al. 2005); while in methods commonly known as *Solid Isotropic Material Penalty* (SIMP), through a constitutive equation, the original stiffness of the solid material, E_0, is multiplied by the density ρ to give the equivalent stiffness of the element as $E = \rho^{\lambda} E_0$, where $0 \leq \rho \leq 1$. The exponent λ is gradually increased starting from 1 in the process of optimization to ensure that the density of each element is close to limit values, *i.e.* zero or one (Rozvany 2001). Using this *power law*, the procedure depends both on λ and also on the finite element mesh used. Some extra constraints, on the perimeter for example, might resolve this dependency.

Many topology optimization methods result in layouts which may be meaningless from a practical point of view, as they yield a large number of small holes or void regions in the domain. To overcome this problem, the designer is forced to introduce a heuristic spatial filter which limits, *e.g.*, the total perimeter of the holes (Rahmatalla and Swan 2004). Thus, the design depends eventually on the filter characteristics. More details on filtering can be found in Sigmund and Petersson (1998), Bourdin (2001), Sigmund (2007).

Associated with many element-based topology optimization techniques is also the checkerboard problem, referring to oscillation between solid and void across elements, due to a possible lack of C^0 continuity of the design variable field. An important recent contribution to overcome this problem is a *node based* algorithm (Rahmatalla and Swan 2003, 2004), where the discretization nodes, not elements, are chosen as design variables; thus the density can vary within each element (Sigmund and Clausen 2007). The method seems to be successful only if a fine mesh is used.

Considering the question of *accuracy* and *efficiency* of topology optimization, not only the optimization procedure itself but also the interplay with the underlying discretization method has to be addressed. Most known approaches use finite elements

of low order—linear triangles or bilinear quadrilaterals—being suitable for the element or node based design variables. Therefore, an increase of accuracy of the finite element approximation can be obtained only by mesh refinement according to the h-version of FEM. As an alternative, the element size, h, can be kept fixed, and convergence is obtained by increasing the polynomial degree p of shape functions locally or globally. During the past two decades, the p-version of FEM has become more and more attractive, and a vast literature is now available on its performance for a large variety of problems. Applications range from linear to nonlinear problems in two and three dimensions, static and dynamic computations and multifield or multiscale simulation in virtually all fields of computational mechanics. For a survey the reader is referred to Szabó et al. (2004).

The major advantage of the p-FEM compared to the h-FEM is its often dramatically higher accuracy for the same computational cost, especially when problems are smooth, *i.e.* no singularities are present in the exact solution to be approximated. For this case, exponential rate of convergence in energy norm can be proved. This can be considered as a first hint that high order elements might be attractive for topology optimization, as—at least in the case of an optimal shape and topology—the stress distribution in the structure should be smooth and thus, no artificial singularities should be present.

Furthermore, high order elements are very robust against locking effects and high aspect ratios. Most important for an application to topology optimization is the ability of high order elements to vary material properties within one element. As high order shape functions demand for high order numerical integration schemes, each integration point can be assigned individual material—the key point for topology optimization in cases the design variables are defined based on units smaller than elements.

In this paper, for the purpose of topology optimization, we use the *Finite Cell Method*, developed recently by the authors (Parvizian et al. 2007; Düster et al. 2008). Instead of generally shaped quadrilateral or hexahedral elements, squares or cubes are used as basic *cells* for the discretization of a (fixed) reference domain containing the (iteratively adjusted) physical domain; hierarchical shape functions are defined on this reference domain. Although the potential of the p-version is fully exploited for high polynomial degrees, in this paper it is also demonstrated that the FCM provides good results even with a relatively low degree, *e.g.* $p = 4$.

The basic idea of the proposed topology optimization algorithm is to strictly separate the discretization of the displacements and that of the geometry. To this end, the Ansatz for the displacement field is defined on a (coarse) finite cell grid, using hierarchical shape functions. Additionally, an independent (fine) material grid is introduced only for geometric description. The material grid defines the material nodes. Using the results of the finite cell method at each iteration, the equivalent stress is determined for each material node. Then, a heuristic criterion determines if the material node should be in the material ($\alpha = 1$) or void ($\alpha = 0$) part of the reference domain. Adjacent material points define a distribution of material by bilinear interpolation and thus control the numerical integration for all finite cells in the next iteration. To consider different meshes, i.e. the finite element mesh, the design variable mesh and the density mesh to represent material distribution has been however considered by other researchers only recently (Nguyen et al. 2010).

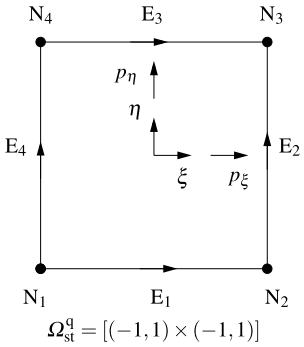

Fig. 2 Standard quadrilateral element: definition of nodes, edges and polynomial degree

The structure of the paper is as follows. Section 2 briefly explains the high order finite element method. The basic ideas of the FCM are given in Sect. 3. Then, Sect. 4 summarizes the optimization procedure, while Sect. 5 starts with a detailed study of the benchmark problem of a cantilever beam to provide an insight how to choose different parameters. Finally, further numerical experiments are presented to demonstrate the robustness and capabilities of the method. For simplicity, we restrict all explanations and examples to two dimensions, although 3D results are already available (Düster et al. 2010).

2 High order approximation

The (two-dimensional) implementation of the p-version is based on a quadrilateral element, using the Ansatz functions introduced by Szabó and Babuška (1991). Figure 2 depicts the standard quadrilateral finite element.

The *tensor product space* (Szabó et al. 2004) is used for definition of the Ansatz functions. It consists of all the polynomials on $\Omega_{st}^{q} = [(-1, 1) \times (-1, 1)]$ spanned by the set of monomials $\xi^i \eta^j$ with $i = 0, 1, \ldots, p_\xi$ and $j = 0, 1, \ldots, p_\eta$. By construction, the two-dimensional shape functions can be classified into three groups:

1. **Nodal modes**

$$N_{1,1}^{\mathrm{N}_i}(\xi, \eta) = \frac{1}{4}(1 + \xi_i \xi)(1 + \eta_i \eta), \quad i = 1, \ldots, 4 \tag{1}$$

   are the standard bilinear shape functions, which are familiar from the isoparametric four-noded quadrilateral element. (ξ_i, η_i) denote the local coordinates of the i-th node. Figure 3 (left-hand side) depicts the mode for node 1.
2. **Edge modes** These modes are defined separately for each individual edge, while they vanish at all other edges. The corresponding modes for edge 1 read:

$$N_{i,1}^{\mathrm{E}_1}(\xi, \eta) = \frac{1}{2}(1 - \eta)\phi_i(\xi) \tag{2}$$

   with $\phi_i(\xi)$ given by (4). Figure 3 (middle) plots the mode for edge 1 with $i = 2$.

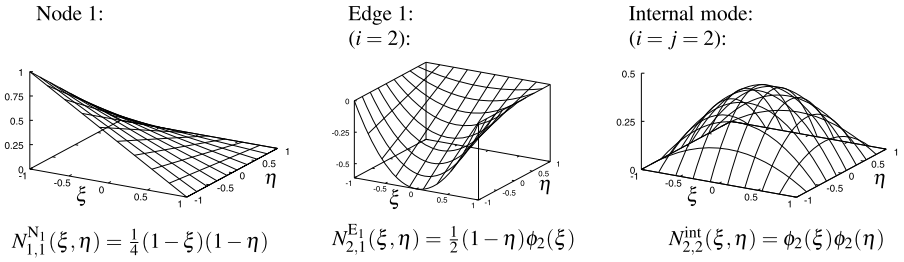

Fig. 3 Examples of hierarchical shape functions for quadrilateral elements

3. **Internal modes**

$$N^{\text{int}}_{i,j}(\xi,\eta) = \phi_i(\xi)\phi_j(\eta) \tag{3}$$

are purely local and vanish at the edges of the quadrilateral element. Figure 3 (right-hand side) depicts the internal mode for $i = j = 2$.

As already indicated, the indices i, j of the shape functions denote the polynomial degrees in the local directions ξ, η. The two-dimensional hierarchic shape functions are based on tensor products of

$$\begin{aligned}\phi_j(\xi) &= \sqrt{\frac{2j-1}{2}}\int_{-1}^{\xi} P_{j-1}(t)\,dt \\ &= \frac{1}{\sqrt{4j-2}}(P_j(\xi) - P_{j-2}(\xi)), \quad j = 2,3,\ldots\end{aligned} \tag{4}$$

where $P_j(\xi)$ are Legendre polynomials

$$P_k(\xi) = \frac{1}{2^k k!}\frac{d^k}{d\xi^k}(\xi^2-1)^k, \quad k = 0,1,\ldots. \tag{5}$$

Crucial for the application of higher order shape functions in the context of topology optimization is their ability to accurately approximate problems where material properties are strongly varying. This will be addressed in the next section where the Finite Cell Method is briefly presented.

3 Finite cell method

The Finite Cell Method (FCM) (Parvizian et al. 2007; Düster et al. 2008) is a combination of a fictitious or embedding domain approach with high order finite element methods. It combines a trivial and thus very fast generation of meshes with high convergence rates. In fictitious domain methods, the original or physical domain is embedded in a geometrically larger domain of a simpler shape. The embedding domain can be readily discretised with structured or Cartesian meshes. Different discretization methods can be applied, ranging from finite difference to finite volume and finite element methods. The name "fictitious domain method" was coined by Saul'ev

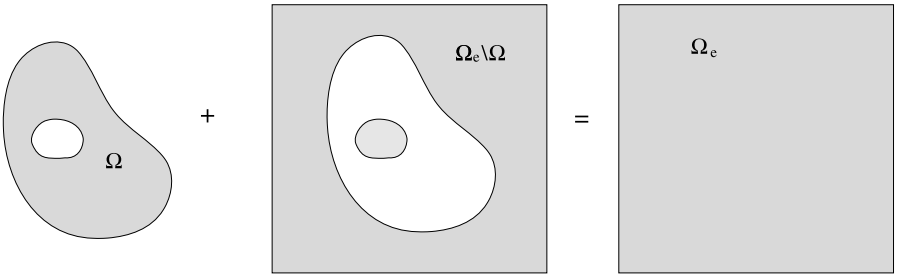

Fig. 4 The domain Ω is extended to Ω_e

(1963) in the early sixties. Since then, many variants of fictitious domain methods have been developed and applied to problems arising in different areas of computational mechanics. For an overview of the huge body of literature, see, for example Ramière et al. (2007), Glowinski and Kuznetsov (2007).

In contrast to classical fictitious domain approaches the FCM uses high order approximation spaces allowing a complex interior structure in each element, which can be cut even by curved boundary of the physical domain. Accurate integration schemes serve to capture both the boundary and possible material discontinuities. To distinguish these geometrically simple yet structurally complex elements from classical finite elements, they are called *cells* and the mesh of all cells is called *finite cell grid*. In fact, the discretization effort is mainly replaced by a more accurate numerical integration.

To be precise, let us begin with the weak formulation of the equilibrium equations of elastostatic problems as

$$\mathcal{B}(\mathbf{u}, \mathbf{v}) = \mathcal{F}(\mathbf{v}) \tag{6}$$

in which

$$\begin{aligned} \mathcal{B}(\mathbf{u}, \mathbf{v}) &= \int_{\Omega} [\mathbf{L}\mathbf{v}]^T \mathbf{C} [\mathbf{L}\,\mathbf{u}]\, d\Omega \\ \mathcal{F}(\mathbf{v}) &= \int_{\Omega} \mathbf{v}^T \mathbf{f}\, d\Omega + \int_{\Gamma_N} \mathbf{v}^T \bar{\mathbf{t}}\, d\Gamma \end{aligned} \tag{7}$$

where $\mathbf{u}$ is the displacement vector, $\mathbf{v}$ the test function, $\mathbf{L}$ the standard strain-displacement operator, $\mathbf{C}$ is the elasticity matrix, $\mathbf{f}$ denotes volume loads and $\bar{\mathbf{t}}$ corresponds to prescribed tractions at the Neumann boundary Γ_N. In (7) Ω denotes the original domain and $\partial\Omega = \Gamma_D \cup \Gamma_N$ represents the boundary with Γ_D denoting the Dirichlet boundary. The original domain Ω is extended to Ω_e that includes also all voids of the domain, such as those appearing while changing the topology, see Fig. 4.

In topology optimization, often the boundaries on which traction and displacements are specified, cannot be changed in the optimization procedure. Therefore, for the purposes of the current paper, the extended domain, Ω_e, is chosen such that the specified Dirichlet and Neumann boundary conditions can be applied at the boundary of Ω_e.

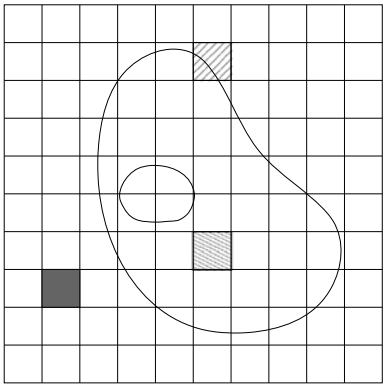

Fig. 5 The extended domain Ω_e is discretised using simple quadrilateral cells

For a more general investigation of boundary conditions, the reader is referred to Parvizian et al. (2007), Düster et al. (2008). Voids or holes are considered as part of the structure 'without material', modeled by a zero-valued elasticity matrix. Thus (6) turns to:

$$\int_{\Omega} [\mathbf{Lv}]^T \mathbf{C}[\mathbf{Lu}]\, d\Omega + \int_{\Omega_e \setminus \Omega} [\mathbf{Lv}]^T \mathbf{0}[\mathbf{Lu}]\, d\Omega = \int_{\Omega} \mathbf{v}^T \mathbf{f}\, d\Omega + \int_{\Omega_e \setminus \Omega} 0 \cdot \mathbf{v}^T \mathbf{f}\, d\Omega + \int_{\Gamma_{e,N}} \mathbf{v}^T \bar{\mathbf{t}}\, d\Gamma \tag{8}$$

or simply,

$$\int_{\Omega_e} [\mathbf{Lv}]^T \alpha \mathbf{C}[\mathbf{Lu}]\, d\Omega = \int_{\Omega_e} \alpha \mathbf{v}^T \mathbf{f}\, d\Omega + \int_{\Gamma_{e,N}} \mathbf{v}^T \bar{\mathbf{t}}\, d\Gamma \tag{9}$$

with

$$\alpha = \begin{cases} 1 & \text{in } \Omega \\ 0 & \text{in } \Omega_e \setminus \Omega \end{cases} \tag{10}$$

The extended domain is now discretised by a mesh of n_c cells being independent of the original domain. For simplicity, it can be assumed that cells Ω_c are quadrilaterals, Fig. 5. The union of all cells forms the extended domain $\Omega_e = \bigcup_{c=1}^{n_c} \Omega_c$.

At the discretised level (9) turns to:

$$\sum_{c=1}^{n_c} \int_{\Omega_c} [\mathbf{Lv}]^T \alpha \mathbf{C}[\mathbf{Lu}]\, d\Omega = \sum_{c=1}^{n_c} \int_{\Omega_c} \alpha \mathbf{v}^T \mathbf{f}\, d\Omega + \sum_{c=1}^{n_c} \int_{\Gamma_{e,N} \cap \Gamma_c} \mathbf{v}^T \bar{\mathbf{t}}\, d\Gamma \tag{11}$$

A standard Bubnov-Galerkin approach yields the following equation system

$$\mathbf{KU} = \mathbf{F} \tag{12}$$

The major difference between (12) and the usual finite element equation is, physically speaking, that not each cell must be filled completely with the material, see Fig. 5. Therefore, in *exterior* cells, containing no material and *hybrid* cells cut by

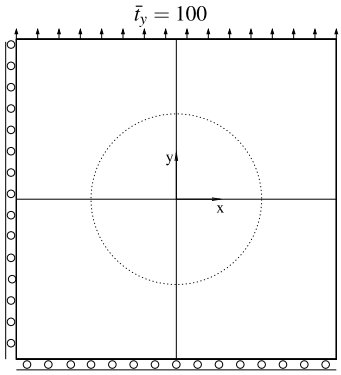

Fig. 6 A perforated plate is discretised by four rectangular cells

the boundary of Ω, the field variable, i.e. the displacement, is not uniquely defined. Yet, *all* extensions of the original solution $\mathbf{u}$ of (6) beyond the boundary of Ω solve (9), as no additional energy is added by those parts of the energy functional, where integration is to be performed outside Ω. Using the best-approximation argument of Galerkin's method, it is concluded from this observation in Parvizian et al. (2007), that the numerical solution of (12) actually approximates a *smooth* extension of $\mathbf{u}$.

To calculate the stiffness matrices, for material cells, $\alpha = 1$, and the usual procedure of integration is applied. In void cells, $\alpha = 0$ and the integration could be bypassed at all. However, a small number, *e.g.* 1×10^{-10} is used for the corresponding terms in the global stiffness matrix to avoid ill-conditioning.

An accurate numerical approximation clearly demands for a precise observation of the boundary of Ω. If low order shape functions are used, allowing only for constant material properties in one element, cut cells need to be small in order to avoid large integration error. If higher order shape functions are used finite cells may even contain voids, and still yield very accurate results. Provided that the numerical integration of cell stiffness matrices is performed accurately, it has been demonstrated in Parvizian et al. (2007), Düster et al. (2008) that exponential convergence rate can be obtained.

To illustrate the performance of the FCM by an example, Fig. 6 shows a linear elastic perforated plate under uniform tension discretised by four quadrilateral cells which do not conform to the geometry of the circular boundary. The reference value for the strain energy is provided by an overkill solution applying a standard p-FEM approach with an exact representation of the curved boundary of the hole. A standard h-version finite element analysis with a low polynomial degree ($p = 1$ or $p = 2$) would result in an algebraic rate of convergence of the error in energy norm. Since the exact solution of this problem is sufficiently smooth, a p-extension on a fixed mesh with high order elements yields an exponential rate of convergence in energy norm, see Fig. 7. The results of the FCM obtained by increasing the polynomial degree of the shape functions of the cell are also plotted in Fig. 7. It is evident that the FCM yields an exponential rate of convergence.

To summarize, a high order polynomial approximation space plus an accurate adaptive integration scheme form the core of the FCM. Voids in the topology optimization procedure will be treated similar to the hole at the center of the plate in this example. For each integration point, the parameter α is calculated using a bilinear interpolation over the material nodes. When $\alpha = 1.0E - 10$, the point is considered

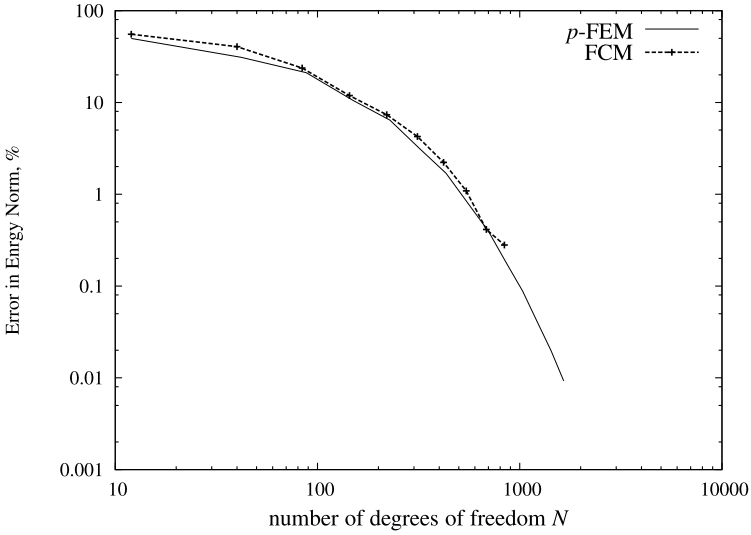

Fig. 7 The relative error in energy norm is plotted versus the degrees of freedom for a p-extension and the FCM

to be in a void, and the corresponding term in the Gauss quadrature can simply be ignored.

4 Topology optimization algorithm

A slightly modified version of the Finite Cell Method is now used for topology optimization, where the boundary of the optimized domain Ω is not known *a priori* but obtained during the iterative optimization process. We apply a heuristic updating algorithm in which α can take values between 0 and 1; this way our algorithm is similar to SIMP. On the other, for the current paper no gradient based optimization algorithm is used, but pointwise values of the von Mises stress are taken to update α. To this end, a refined *material grid* composed of *material cells* is applied, providing a piecewise bilinear interpolation of α defined at the *material nodes*, see Fig. 8. This approach avoids introducing singularities which otherwise could be expected when removing a material cell. If the stress in the remaining material exceeds a permissible limit it is possible to recover the material by increasing the value of α for neighboring material nodes.

Note that, in general, the material grid is not conforming to the grid of finite cells. Whereas the finite cell grid is the basis for defining shape functions, the (independent) material grid is used to describe the shape of Ω during the optimization process. Therefore, the geometric description (or equivalently material density) is completely separated from the discretization of the displacement field and the resolution of each quantity (geometry/material and displacement field) can be adjusted separately. To emphasize, the key advantage of the proposed method lies in the fact that, by applying a bilinear interpolation over a fine material grid, the scale of design variables

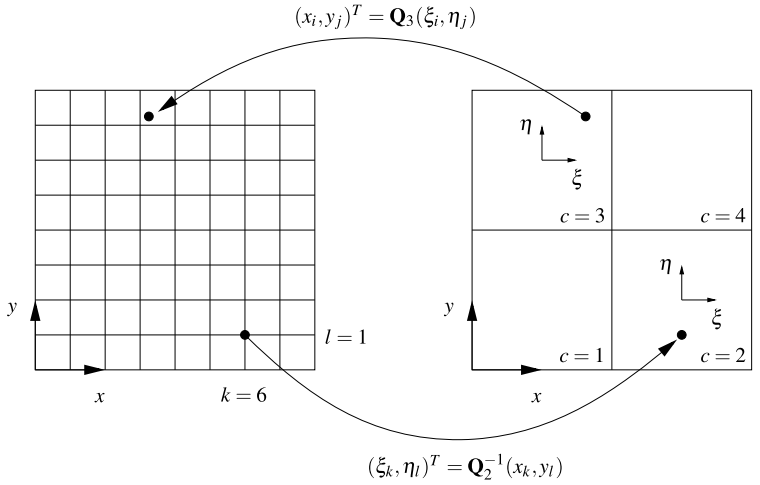

Fig. 8 8×8 material grid (*left-hand side*), and independent finite cell grid with 2×2 cells

is reduced from large cells to small supporting areas (the material cells) and their material nodes.

In Fig. 8 an example for a material grid and a finite cell grid is depicted, both defined on the embedding domain Ω_e. Information concerning the geometry/density of material is related to the 8×8 material grid. For each material node, two values are stored: $\alpha > 0$ which defines the material density and β which can be either 0 or 1. The latter quantity determines whether for a node α is fixed or it can be changed. This enables the user to define regions which remain either material or void during the optimization procedure.

Based on the equivalent stress σ^{vm} computed at each material node, the corresponding α is changed according to

$$\alpha = \left(\frac{\sigma^{vm}}{\sigma^{obj}} \right)^{\rho} \tag{13}$$

in which σ^{obj} is the objective stress and $\rho > 1$ is a numerical parameter still to be defined. If $\sigma^{vm} < \sigma^{obj}$, then the material is weakened by the factor α. If $\sigma^{vm} > S.F. \times \sigma^{obj}$, where $S.F. > 1$ is a user-defined stress factor to control the upper limit, then the von Mises stress at the material node is considered as too high. In the absence of singularities, this indicates that more material is necessary in this neighborhood to carry the high stresses. Therefore the α value of adjacent material nodes is set to 1 in order to reduce the stress level. At most for two additional material nodes, one on the top or the bottom, and one on the left or right, α is modified. Apparently, the material node with smaller α in each direction, as shown in Fig. 9, is the mechanically motivated reasonable choice. This ensures that the algorithm is not locked into a highly stressed region and can expand the material domain if necessary to carry the load.

Therefore the *alpha* value of adjacent material nodes is set to 1 in order to reduce the stress level.

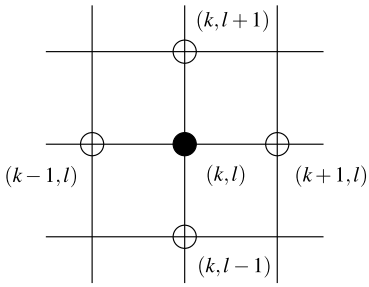

Fig. 9 Each material node (k,l) is surrounded by four adjacent nodes. If the von Mises stress is too high at node (k,l), then $\alpha = 1$ is set on the *left* or *right*, also either on the *top* or *bottom* neighbor. Therefore, at most two of the four neighbors will—in addition to the node (k,l) itself—be set to $\alpha = 1$

Algorithm A.1 Topology optimization algorithm using the FCM and a material grid

1: Define the embedding domain Ω_e, boundary conditions, objective stress σ^{obj}
2: Generate uniform material grid and initialize values $\alpha_{k,l}$ and $\beta_{k,l}$ for all nodes
3: Generate structured finite cell grid
4: $i = 0$
5: **repeat**
6: $i = i + 1$
7: **Perform a finite cell computation**
8: **for all** material nodes **do**
9: **1. evaluate** $\alpha^i_{k,l}$ **according to** (13)
10: **2. modify** $\alpha^i_{k,l}$ **according to stress concentrations**
11: **if** $\sigma^{vm}_{k,l} > S.F. \times \sigma^{obj}$ **then**
12: set $\alpha^i_{k,l} = 1$ also for adjacent material nodes (see Fig. 9)
13: **end if**
14: **3. restrict** $\alpha^i_{k,l}$ **to** $[\alpha_{\min}, 1]$
15: **end for**
16: **until** $((\|\alpha^i_{k,l} - \alpha^{i-1}_{k,l}\| < TOL)$ or $(i >$ maximum number of iterations$)$)

At the last step, any $\alpha > 1$ is replaced by $\alpha = 1$, and any $\alpha < \epsilon$ is set to $\alpha = \alpha_{\min} = 10^{-10}$, in which ϵ is a small tolerance like 10^{-8}. The algorithm results in a design in which the von Mises stress at any point is in the acceptable range of $\sigma^{obj} \leq \sigma^{vm} \leq S.F. \times \sigma^{obj}$ except for inherent singularities at supporting corners for example. The procedure stops when the change of the $\alpha_{k,l} = \alpha(x_k, y_l)$ values between two consecutive steps is less than a prescribed tolerance or the maximum number of iterations is exceeded. The algorithm is summarized in Algorithm A.1.

During the iteration of the topology optimization algorithm, the stiffness matrices

$$\begin{aligned}\mathbf{K}_c &= \int_\eta \int_\xi \mathbf{B}_c^T(\xi,\eta)\alpha(\mathbf{x}(\xi,\eta))\mathbf{C}\mathbf{B}_c(\xi,\eta)\det\mathbf{J}_c\, d\xi\, d\eta \\ &= \sum_{sc=1}^{n_{sc}} \int_s \int_r \mathbf{B}_c^T(\xi(r,s),\eta(r,s)) \\ &\quad \times \alpha(\mathbf{x}(\xi(r,s),\eta(r,s)))\mathbf{C}\mathbf{B}_c(\xi(r,s),\eta(r,s))\det\mathbf{J}_c\det\tilde{\mathbf{J}}_c^{sc}\, dr\, ds \end{aligned} \tag{14}$$

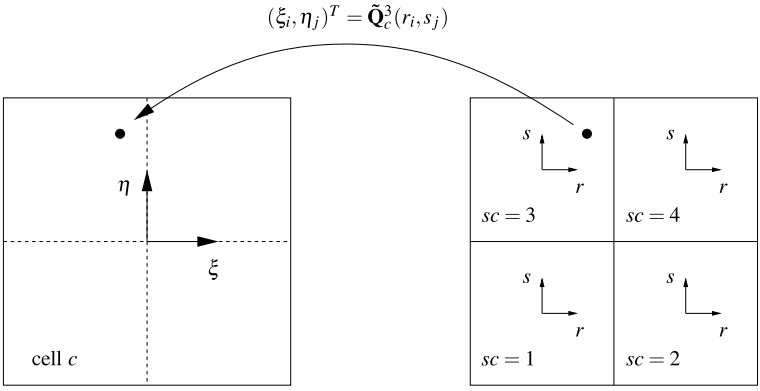

Fig. 10 A cell is subdivided into 2×2 sub-cells for integration purposes

of the $c = 1, \ldots, n_c$ cells need to be computed. In (14) $\mathbf{B}_c$ denotes the standard strain-displacement matrix and, due to the rectangular shape of the cell, $\mathbf{J}_c = \text{grad}^T \mathbf{Q}_c(\xi, \eta)$ denotes the constant Jacobian matrix. To accurately compute the stiffness matrix, cell c is subdivided into a uniform grid of n_{sc} *integration cells* or *sub-cells* for integration purposes only. These sub-cells should not be confused with the material cells. An additional mapping function $(\xi, \eta)^T = \tilde{\mathbf{Q}}_c^{sc}(r, s)$ from the local coordinates (r, s) of the sub-cell sc to the local coordinates (ξ, η) of the cell c is introduced, resulting in the additional (constant) Jacobian matrix $\tilde{\mathbf{J}}_c^{sc} = \text{grad}^T \tilde{\mathbf{Q}}_c^{sc}$. On each of the n_{sc} sub-cells a standard Gaussian quadrature is performed to integrate the corresponding part of the stiffness matrix of cell c, see Fig. 10.

The accuracy of the integration can be controlled by either increasing the number of sub-cells or the number of Gaussian points in each sub-cell or by a combination of both. Since the integrand of cells broken by the boundary is discontinuous, an increase of the number of sub-cells is of advantage avoiding oscillations which would occur when choosing a small number and a high integration order. The integration of the cells is carried out in an adaptive approach, applied in two steps.

In the first step the integration error is estimated. To this end, the integration order is fixed and the number of sub-cells is increased until the *change of the computed area* (or volume) of the broken cell is less then a pre-defined threshold. This approach is computationally very cheap. Once the number of sub-cells is adaptively determined, in a second step the stiffness matrix is integrated.

The material density α is computed according to (13) for each integration point. To this end, the location of the Gaussian point (r_i, s_j) defined in the local coordinates of the sub-cell is mapped to the local coordinates of the cell (ξ_i, η_j) and from there into the global coordinate system (x, y). We apply linear mapping functions, i.e $(\xi, \eta)^T = \tilde{\mathbf{Q}}_c^{sc}(r, s)$ and $(x, y)^T = \mathbf{Q}_c(\xi, \eta)$ to compute the change of variables, see Figs. 8 and 10. As a structured material grid is used, the corresponding material cell containing the integration point under consideration can be readily determined. To finally obtain the value of $\alpha(\mathbf{x}(\xi_i(r_i, s_j), \eta_j(r_i, s_j)))$, a bilinear interpolation from the four surrounding material nodes is performed. The mapping of a Gaussian point (of cell $c = 3$) is exemplarily sketched in Fig. 8.

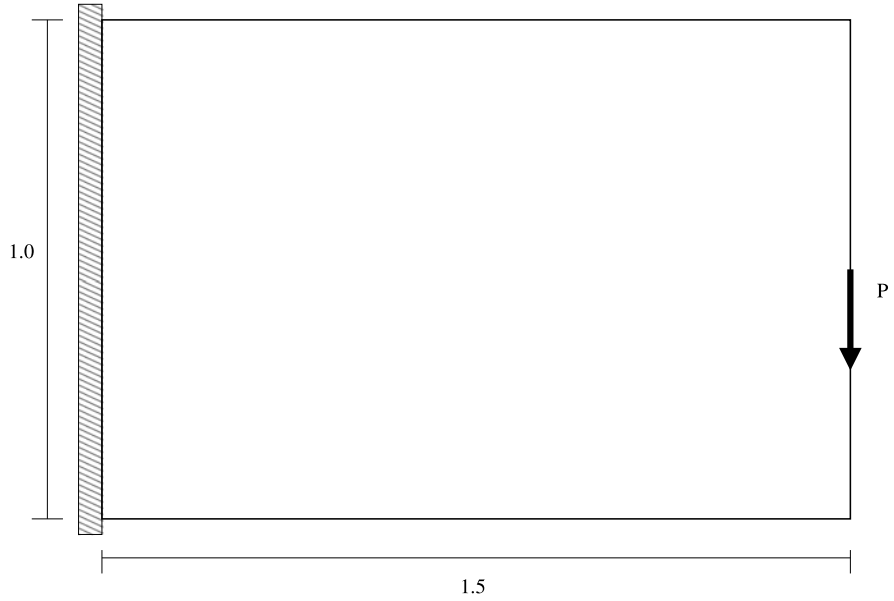

Fig. 11 The cantilever beam is discretised using 42×33 cells

Having computed all cell stiffness matrices and the solution of the resulting mechanical system, in a post-processing step the stresses and, based on (13), a new value for $\alpha_{k,l}$ is computed for all nodes (x_k, y_l) of the material grid. Inverse mapping functions are used now, which are linear due to the Cartesian nature of all used grids. The situation is exemplarily depicted in Fig. 8, where (x_6, y_1) lies in cell $c = 2$.

5 Numerical examples

5.1 Cantilever beam

In this section, several numerical examples are provided to demonstrate the performance of the method. In all examples, the material used is steel with $E = 206.9$ GPa, and $\nu = 0.29$. Examples presented here are solved using AdhoC, which is a h and p-version finite element code (Düster et al. 2004) modified for the finite cell formulation. Paraview is used for post-processing aims.[1]

The optimum solution achieved by an algorithm is subject to the set of parameters chosen, as well the filtering scheme. Therefore, it is difficult to compare quantitatively the outcome of different approaches; although each approach may converge to a solution which, only within its defined measures, is optimum.

As a first example we investigate a cantilever beam, which has frequently been used as a benchmark problem for topology optimization algorithms. Figure 11 shows

[1] See http://www.paraview.org.

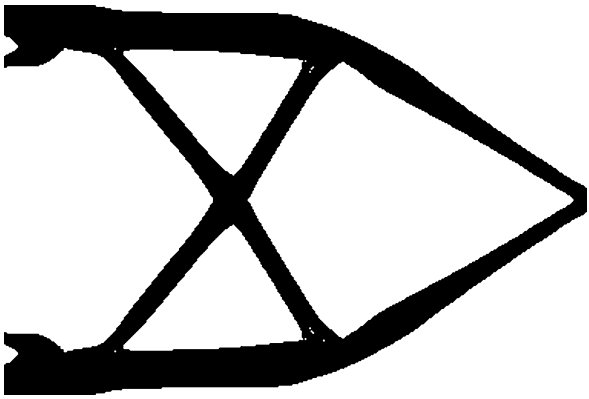

Fig. 12 $\sigma^{obj} = 25$, $\rho = 3$, $p = 15$, $n_{gp} = 16 \times 16$, iteration step 40

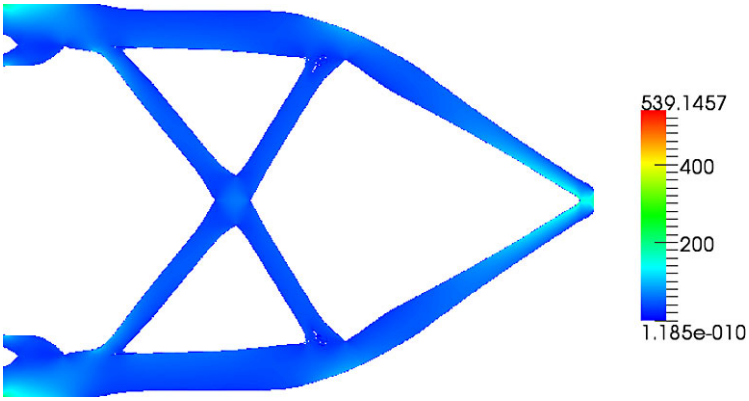

Fig. 13 von Mises stress distribution for the reference solution shown in Fig. 12

the initial configuration. The beam is discretised using 1386 finite cells. The load is a uniform traction applied at the mid-cell of the right-hand side of the beam. The under-traction boundary is not subject of any change through the optimization procedure. For description of the domain Ω, the resolution of the material grid used is 1500×1000. Note that the material grid and finite cell mesh are intentionally chosen so that nodes do not match. A high order Gaussian integration is necessary to approximate the discontinuous material. To improve the numerical integration, each cell is divided to sub-cells if necessary. The required number of sub-cells is determined adaptively as prescribed in Sect. 4.

The objective von Mises stress is set to $\sigma^{obj} = 25$ MPa. To produce a reference solution, the solution is computed with $p = 15$ and $n_{gp} = 16 \times 16$ Gaussian integration points in each sub-cell. The final material distribution of the converged topology optimization is depicted in Fig. 12.

Figure 13 shows the von Mises stress distribution in the beam. High stresses occur only at the supporting regions, and throughout the domain the stress is distributed very smoothly. Figure 14 shows that there is no artificial singularity induced in the problem even at the tip when two levers meet.

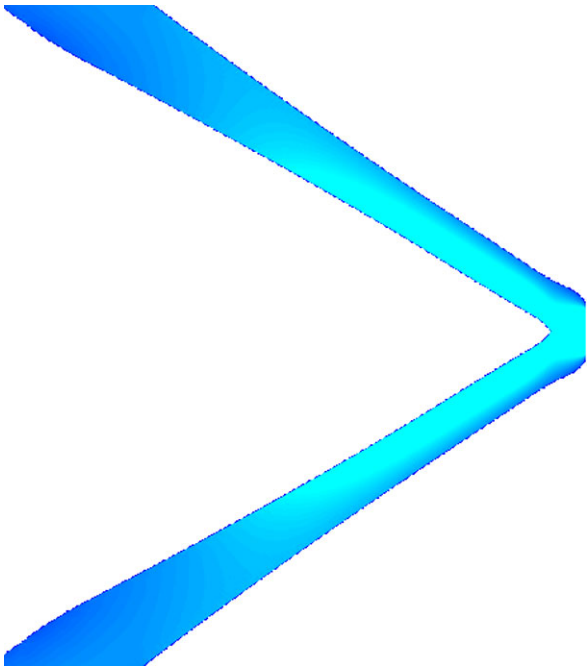

Fig. 14 von Mises stress distribution at the tip of the reference beam shown in Fig. 12

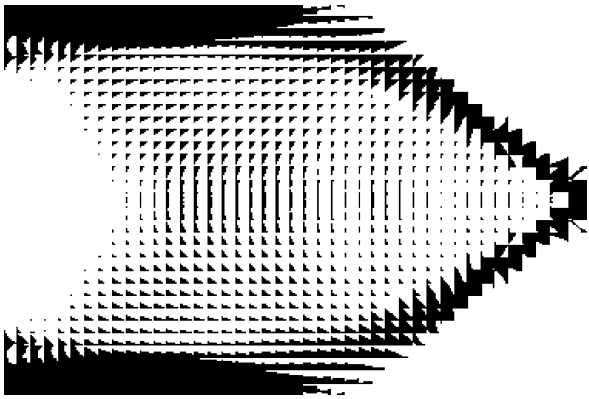

Fig. 15 Checkerboard pattern for $p = 1$

To examine the robustness of the method by changing computational parameters, let us start with low order elements, *e.g.* a polynomial degree of $p = 1$, yet with the same high resolution of the material grid as before. The checkerboard pattern in Fig. 15 indicates, that the poor approximation property of low order elements is the source for an unphysical solution.

Next, the influence of the quality of the spatial discretization is studied. Figure 16 shows the result for $p = 3$ and $n_{gp} = 4 \times 4$ Gaussian points per sub-cell while the resolution of the material grid is 300×200. For the same material grid, Fig. 17 shows the result for $p = 6$. Comparing Figs. 17 (300×200 grid) and 12 (1500×1000 grid)

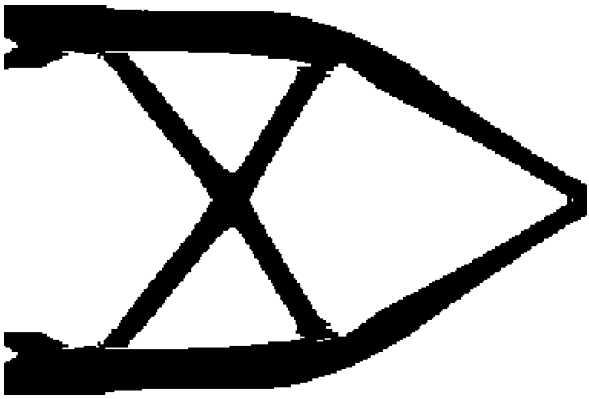

Fig. 16 $p = 3$, material grid 300×200

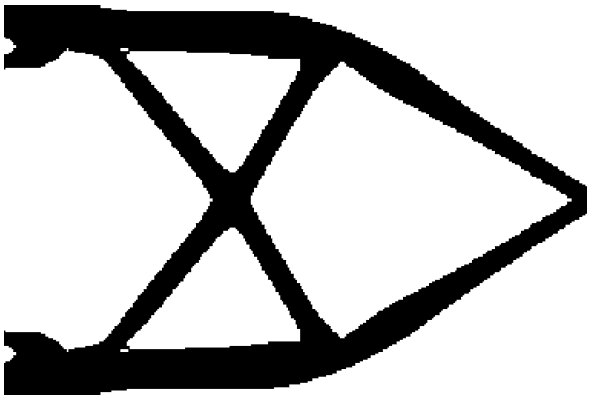

Fig. 17 $p = 6$, material grid 300×200

indicates, that a finer material grid is only necessary if more details of the stress distribution or a smoother boundary is demanded.

Figure 18 demonstrates the convergence behavior of the algorithm in reducing the area (weight) of the beam, for the problem defined in Fig. 17. After only 10 iterations, convergence is obtained.

To demonstrate that the algorithm does not produce checkerboarding with a different settings, a longer beam is now considered while $\sigma^{obj} = 45$. Figure 19 presents the result. In many more 2D and 3D examples, never any filtering has been applied in the present algorithm, yet never checkerboarding was observed, provided that the polynomial degree was high enough.

To illustrate the capability of the algorithm to exclude specified regions from the optimization procedure, the cantilever beam, Fig. 11, is considered again. For practical reasons, such as piping, a specific region must often be kept as void. Figure 20 gives the details. Therefore $\alpha = 0$ is fixed for nodes that are within the circular hole. Figure 21 shows the result. It is interesting to note that both the finite cell grid and the material grid are relatively coarse. A smoother boundary can be achieved if only a finer material grid is used. The general configuration however remains the same.

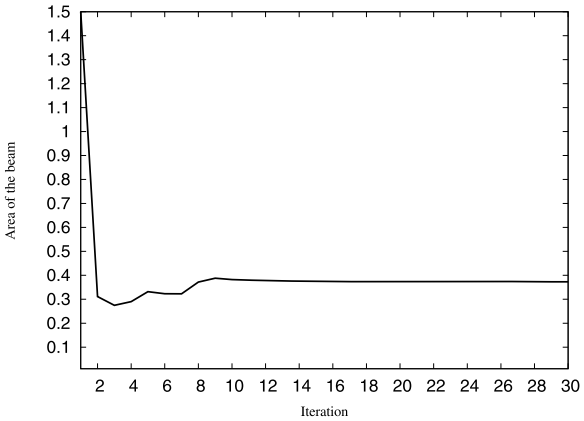

Fig. 18 Convergence of the area plotted against iteration step

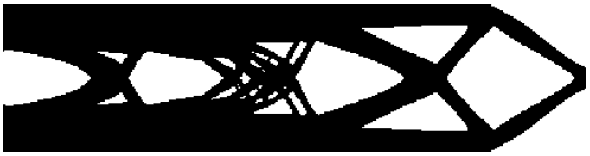

Fig. 19 A beam with dimension 4×1 is discretised using 1564 cells, and a material grid of 800×200, $p = 10$, and the objective stress is $\sigma^{obj} = 45$

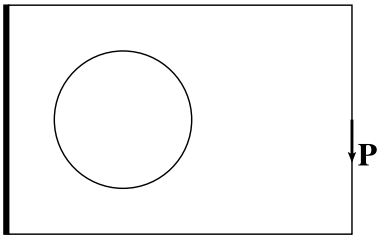

Fig. 20 A perforated beam with dimension 1.5×1 discretised using 384 cells. The circular hole is at (0.5, 0.5) and its radius is 0.3

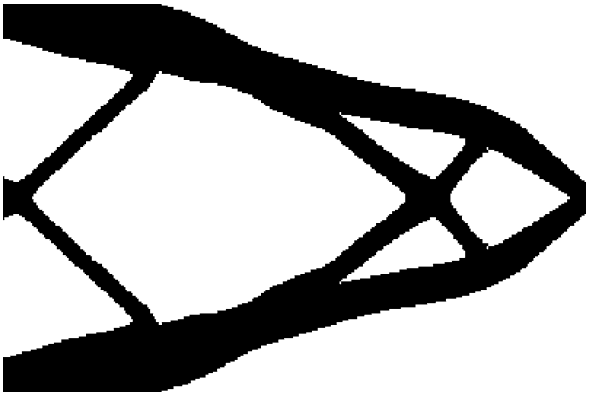

Fig. 21 The perforated beam; material grid is 150×100, $p = 10$, and the objective stress is $\sigma^{obj} = 25$

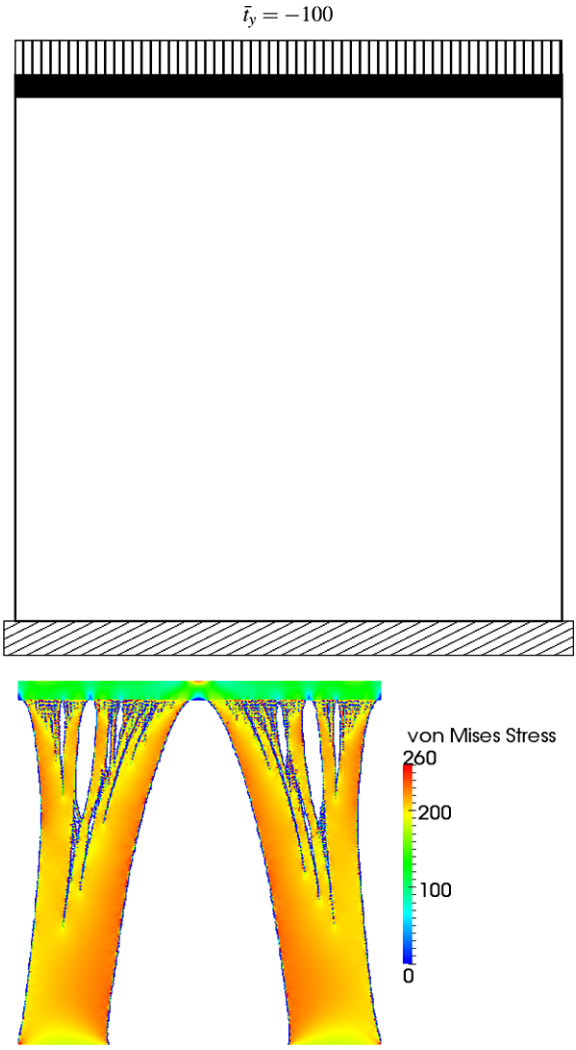

Fig. 22 σ^{obj}=180, $S.F. = 1.4$ domain: 1×1, 40×40 uniform cells, $p = 5$, material grid: 200×200

5.2 Bridge

Initial geometry and boundary conditions of this problem are defined in Fig. 22 (upper part). The bridge like structure is subject to a uniformly distributed load applied on the upper stiff platform. The optimized design is strongly depending on the objective stress and the stress factor. The chosen parameters are listed in the caption of Fig. 22.

As shown in the lower part of the figure, the stress at any point but the singular corners is within the chosen limits. Since in the first few iterations, a large part of the material is removed and the stress level in the remaining part passes the permissible limit, the recovering procedure takes more material into such regions. This is essential to obtain an admissible solution.

5.3 Discussion of the numerical examples

Like in any optimization algorithm, different parameters have interacting effects. Our numerical tests show that for $p < 3$ the results are very often not acceptable. Yet, starting from $p = 4$ the convergence of the optimization algorithm is good and the results are physically reasonable. With increasing polynomial degrees the stress distribution of the optimized structures gets smoother and smoother, and a consecutive increase of the polynomial degree leaving all other parameters unchanged can be used to judge the stability of the optimized solution. Yet, we observed for a large number of numerical examples that the general layout of the structure did not change significantly for polynomial degrees beyond 5.

Although different values of ρ were also investigated, in all numerical tests performed $\rho = 3$ was a good choice. The size of the material grid proved to have no major effect on the final configuration as long as the grid is relatively finer than the finite cell mesh. Finer grids will represent smoother boundaries in the final design, yet a finer material grid may also reveal relatively small low stressed regions, which might be ignored when the grid is coarse and which are not relevant from a practical point of view. The number of cells has a considerable effect on the approximate solution. High order polynomial shape functions allow using relatively coarse cells. For the cantilever beam, similar result as those shown in this paper can be achieved by only 160 cells, and a material grid of 300×200.

In the presented examples element instabilities did not emerge; therefore the need for filtering is not triggered. However, better looking results can be expected if suitable filtering is included. As far as mesh-independency is concerned, in the FCM, the mesh is just a rectangular mesh, and the result depends rather on the order of the approximation Ansatz, and the integration scheme.

Unlike similar approaches in topology optimization, the outcome of the presented algorithm is black and white. This can be explained by the nature of the algorithm which keeps even small part of an element as material and removes it if the stress is lower than the specified object. Therefore, there are no in-between densities.

6 Conclusions

The main feature of topology optimization using the Finite Cell Method is in providing the possibility to separate the design space from the approximation space and thus to use a material description which is strongly refined compared to the scale of the computational mesh. A key point for this method is the use of high order shape functions for approximating the displacement field. As demonstrated by examples, artificial singularities in the stress field are completely avoided and very accurate stress distribution are obtained. Furthermore, despite filtering was not applied, checkerboarding was never observed in any of the vast numerical experiments for polynomial degrees $p > 3$. With a moderately high polynomial degree ($p > 4$) mechanically acceptable results could be obtained in all test cases.

The heuristic optimization algorithm taken here for simplicity of description is not the only algorithm that could be combined with the FCM. It is expected that the

performance of the method is even improved if more advanced optimization procedures like gradient-based methods are used, yet no principle differences in the general observations are expected.

Acknowledgement The authors would like to thank Professor Kai-Uwe Bletzinger and Professor Ole Sigmund for their valuable hints and comments.

References

Allaire G, Jouve F, Toader A (2004) Structural optimization using sensitivity analysis and a level-set method. J Comput Phys 194/1:363–393

Allaire G, Jouve F (2006) Coupling the level set method and the topological gradient in structural optimization. Solid Mech. Appl. 137/1:3–12

Andreassen E, Clausen A, Schevenels M, Lazarov BS, Sigmund O (2010) Efficient topology optimization in MATLAB using 88 lines of code. Struct Multidiscip Optim. doi:10.1007/s00158-010-0594-7

Bendsøe MP (1995) Optimization of structural topology, shape and material. Springer, Germany, pp 136–137

Bendsøe MP, Sigmund O (2004) Topology optimization, theory, methods, and applications. Springer, Berlin

Bendsøe MP, Lund E, Olhoff N, Sigmund O (2005) Topology optimization—broadening the areas of application. Control Cybern 34(1):7–35

Bourdin B (2001) Filters in topology optimization. Int J Numer Methods Eng 50:2143–2158

Challis JV (2010) A discrete level-set topology optimization code written in Matlab. Struct Multidiscip Optim 41:453–464

Düster A, Bröker H, Heidkamp H, Heißerer U, Kollmannsberger S, Krause R, Muthler A, Niggl A, Nübel V, Rücker M, Scholz D (2004) AdhoC^4—user's guide. Lehrstuhl für Bauinformatik, Technische Universität München

Düster A, Parvizian J, Yang Z, Rank E (2008) The finite cell method for three-dimensional problems of solid mechanics. Comput Methods Appl Mech Eng 197:3768–3782

Düster A, Parvizian J, Rank E (2010) Topology optimization based on the finite cell method. Proc Appl Math Mech 10:151–152

Eschenauer HA, Olhoff N (2001) Topology optimization of continuum structures: a review. Appl Mech Rev 54(4):331–390

Eschenauer HA, Kobelev HA, Schumacher A (1994) Bubble method for topology and shape optimization of structures. Struct Optim 8:142–51

Glowinski R, Kuznetsov Y (2007) Distributed Lagrange multipliers based on fictitious domain method for second order elliptic problems. Comput Methods Appl Mech Eng 196:1498–1506

Huang X, Xie YM (2008) A new look at ESO and BESO optimization methods. Struct Multidiscip Optim 35:89–92

Huang X, Xie YM (2010) A further review of ESO type methods for topology optimization. Struct Multidiscip Optim 41:671–683

Huang X, Xie YM (2010) Evolutionary topology optimization of continuum structures with an additional displacement constraint. Struct Multidiscip Optim 40:409–616

Le C, Norato J, Bruns T, Ha C, Tortorelli D (2010) Stress-based topology optimization for continua. Struct Multidiscip Optim 41:605–620

Nguyen TH, Paulino GH, Song J, Le CH (2010) A computational paradigm for multiresolution topology optimization (MTOP). Struct Multidisc Optim 41:525–539. doi:10.1007/s00158-009-0443-8

Parvizian J, Fenner RT (1997) Shape optimization by the boundary element method: a comparison between mathematical programming and normal movement approaches. Eng Anal Bound Elem 19:137–145

Parvizian J, Düster A, Rank E (2007) Finite cell method: h- and p-extension for embedded domain problems in solid mechanics. Comput Mech 41:121–133

Rahmatalla S, Swan CC (2003) Form finding of sparse structures with continuum topology optimization. J Struct Eng 129(12):1707–1716

Rahmatalla S, Swan CC (2004) A Q4/Q4 continuum structural topology optimization implementation. Struct Multidiscip Optim 27:130–135

Ramière I, Angot P, Belliard M (2007) A fictitious domain approach with spread interface for elliptic problems with general boundary conditions. Comput Methods Appl Mech Eng 196:766–781
Rozvany GIN (2001) Aims, scope, methods, history and unified terminology of computer-aided topology optimization in structural mechanics. Struct Multidiscip Optim 21:90–108
Saul'ev VK (1963) On solution of some boundary value problems on high performance computers by fictitious domain method. Sib Math J 4:912–925
Sethian JA, Wiegmann A (2000) Structural boundary design via level set and immersed interface methods. J Comput Phys 163:489–528
Sigmund O (2007) Morphology-based black and white filters for topology optimization. Struct Multidisc Optim 33:401–424
Sigmund O, Petersson J (1998) Numerical instabilities in topology optimization: a survey on procedures dealing with checkerboards, mesh-dependencies and local minima. Struct Optim 16:68–75
Sigmund O, Clausen PM (2007) Topology optimization using a mixed formulation: an alternative way to solve pressure load problems. Comput Methods Appl Mech Eng 196:1874–1889
Szabó BA, Babuška I (1991) Finite element analysis. Wiley, New York
Szabó BA, Düster A, Rank E (2004) The p-version of the finite element method. In: Stein E, de Borst R., Hughes TJR (eds) Encyclopedia of computational mechanics, vol 1. Wiley, New York, pp 119–139
Tang X, Bassir DH, Zhang W (2010) Shape sizing optimization and material selection based on mixed variables and genetic algorithm. Optim Eng. doi:10.1007/s11081-010-9125-z
Zhou M, Rozvany GIN (2001) On the validity of ESO type methods in topology optimization. Struct Multidisc Optim 21:80–83
Xie YM, Steven GP (1997) Evolutionary structural optimization. Springer, London, pp 12–29